

Ba-Fe titanates in peralkaline granite of the Ilímaussaq Complex, South Greenland

MAŁGORZATA CEGIEŁKA^{1,2,*}, BOGUSŁAW BAGIŃSKI¹, RAY MACDONALD^{1,3},
BEATA MARCINIAK-MALISZEWSKA¹ and MARCIN STACHOWICZ¹

¹ Department of Geochemistry, Mineralogy and Petrology, Faculty of Geology, University of Warsaw,
ul. Żwirki i Wigury 93, 02-089 Warsaw, Poland.

E-mails: B.Baginski1@uw.edu.pl; b.maliszewska@uw.edu.pl; marcin.stachowicz@chem.uw.edu.pl

² Institute of Geological Sciences, Polish Academy of Sciences, Research Centre in Warsaw,
Twarda 51/55, 00-818 Warsaw, Poland.

E-mail: m.cegielka@twarda.pan.pl

³ Environment Centre, Lancaster University, Lancaster LA1 4YQ, UK.

E-mail: raymacdonald186@gmail.com

* Corresponding author

ABSTRACT:

Cegielka, M., Bagiński, B., Macdonald, R., Marciniak-Maliszewska, B. and Stachowicz, M. 2022. Ba-Fe titanates in peralkaline granite of the Ilímaussaq Complex, South Greenland. *Acta Geologica Polonica*, **72** (1), 1–8.

A peralkaline granite of the Ilímaussaq Complex, South Greenland, contains the rare mineral henrymeyerite $[(\text{Ba}_{0.92}\text{Na}_{0.05}\text{Ca}_{0.03})_{1.0}(\text{Ti}_{6.87}\text{Fe}^{2+}_{1.04}\text{Nb}_{0.03})_{7.9}\text{O}_{16}]$, a low-Fe Ba titanate $[(\text{Ba}_{0.74}\text{Ca}_{0.02}\text{Na}_{0.05})_{0.8}(\text{Ti}_{4.90}\text{Fe}^{2+}_{0.15}\text{Nb}_{0.04})_{5.1}\text{O}_{11}]$, and an unidentified Ba titanosilicate. Both titanates show the coupled substitution $2\text{Na}^{+} + \text{Si}^{4+} \rightarrow \text{Ba}^{2+} + \text{Ti}^{4+}$. The minerals are present as tiny crystals fringing ilmenite inclusions in an amphibole crystal and are thought to have formed during the hydrothermal stage of the granite's evolution.

Key words: Ilímaussaq peralkaline granite; Henrymeyerite; Low-Fe Ba Titanate.

INTRODUCTION

Henrymeyerite $[\text{Ba}(\text{Ti}^{4+}\text{Fe}^{2+})_8\text{O}_{16}]$ is a member of the priderite group of the hollandite supergroup of minerals (Biagioni *et al.* 2013). From its first recognition in a mineralised vug in a carbonatite vein of the Kovdor alkaline ultramafic complex, Russia (Mitchell *et al.* 2000), it has been recorded in a few further localities, including the Crazy Mountains, Montana, USA (Chakhmouradian and Mitchell 2002), the Khibiny Massif, Kola Peninsula, Russia (Mikhailova *et al.* 2007), and Šebkovice, Czech Republic (Krmíček *et al.* 2011). However, as noted by Mitchell *et al.* (2000), some pre-2000 reports have typically referred to it under such names as Ba-Fe hollandite-type titanates (Mitchell and Bergman 1991) or Ba-Fe-hollandite (Platt 1994; Chakhmouradian and Mitchell 1999).

So far as we know, henrymeyerite has been found only in silica-undersaturated parageneses. In this paper, we describe it in a peralkaline granite from the Ilímaussaq complex, South Greenland, where it is associated with what appears to be the most Fe-poor Ba titanate yet reported. It is also closely associated with a Ba titanosilicate with an unusually high Ti/Si ratio (~3) which we still have not identified. This note provides compositional data on all three phases.

GEOLOGICAL SETTING

Dated at 1161 ± 5 Ma (Krumrei *et al.* 2006), the complex, situated within the Younger Gardar southern rift zone (Upton 2013), is one of the youngest in the Gardar Igneous Province. The pressure of em-

placement has been estimated as c. 1 kbar (Marks *et al.* 2003). The complex comprises three separate intrusions (Nielsen and Steenfelt 1978; Steenfelt 1981). In order of emplacement these intrusions are: (1) An augite syenite stock with an ovoidal plan measuring c. 19 × 9 km. The syenites are slightly silica-undersaturated, with nepheline as a minor component. (2) Quartz syenites and peralkaline granites cropping out over an area of c.16 km² in the highest parts of the complex. (3) Silica-undersaturated syenites (pulsakites, foyaites and sodalite foyaite) that occupy the greater part of the exposed complex. These crystallized consecutively downwards and form the roof zone to the third intrusion. The peralkaline granite is holocrystalline, porphyritic and massive without any visible orientation of crystals. The dominant mineral is subhedral perthitic feldspar (54 modal %; 2–4 mm). The potassic feldspar composes 26% of the granite; the bulk composition is Or_{98.43}Ab_{1.57}. The sodic feldspar, making up 29% of the granite, is albite with an average composition of Ab_{99.52}Or_{0.41}An_{0.07}. Both types of feldspar contain aegirine inclusions ranging in size from 5 to 30 μm. These are probably the cause of the remarkable green colour of the rock. Anhedronal quartz, often showing undulose extinction, forms over 35% of the granite, the grain size ranging from 60 μm to 5 mm. Amphiboles are the most abundant mafic minerals (8 modal %), forming large (40 μm to 6 mm) crystals with a zonation ranging from deep reddish-brown, katophoritic cores to dark bluish-green, arfvedsonitic margins. Commonly it is replaced by aegirine. Aenigmatite occurs as deep-brown anhedronal crystals, up to 3 mm in size, commonly mantled by aegirine, titanite and fluorite; the average formula is (Na_{3.94}Ca_{0.08})_{4.02}Ti_{1.93}(Fe²⁺_{10.10}Mn_{0.20})_{10.30}Si_{11.73}O₄₀. Our sample of the granite contains the following accessory minerals, which total ~1 modal %: aegirine, astrophyllite, britholite-(Ce), catapleite, chevkinite-(Ce), ekanite, elpidite, fluorite, henrymeyerite, Fe-poor Ba-titanate, ilmenite, leucosphenite, lorenzenite, monazite-(Ce), narsarsukite, neptunite, pectolite, pyrochlore, thorite, titanite, zircon, and five unidentified phases. Fluorite is the most abundant accessory mineral, comprising ~0.2 modal % of the whole-rock.

ANALYTICAL METHODS

Our sample was collected from a loose block in the River Dyrnaes. From its intense green colour and mineralogy, the sample is undoubtedly from the Ilímaussaq peralkaline granite, the so-called Green

	wt. %		ppm		ppm		ppm
SiO ₂	73.35	Ba	51	Th	29.8	Ho	4.53
TiO ₂	0.21	Be	24	U	7.7	Er	12.3
Al ₂ O ₃	10.85	Co	36.5	V	<8	Tm	1.67
Fe ₂ O ₃ *	4.38	Cs	2.50	W	558	Yb	10.16
MnO	0.09	Ga	35.6	Zr	572	Lu	1.39
MgO	0.04	Hf	14.7	La	174	Y	142
CaO	0.52	Nb	140	Ce	341		
Na ₂ O	4.55	Ni	<20	Pr	37.6		
K ₂ O	4.84	Rb	454	Nd	138		
P ₂ O ₅	0.02	Sc	<1	Sm	24.6		
LOI	0.8	Sn	10.0	Eu	1.31		
TOT/C	0.14	Sr	20.2	Gd	21.7		
Total	99.79	Ta	13.1	Dy	21.3		

Table 1. Chemical composition of the Green Granite. Fe₂O₃* – all Fe as Fe³⁺.

Granite (Table 1). Mineral analyses were made on a single thin section of the granite, which was initially studied with polarized light microscope NIKON ECLIPSE LV100 POL, equipped with a high-precision automatic stage. Both plane and crossed polarized light images of minerals and textures present in the granite were acquired. Quantitative element distribution maps and point analyses were acquired using a Zeiss SigmaTM VP FE (field emission) – SEM equipped with new generation SDD-type two EDS (XFlash 6|10TM) detectors produced by Bruker. Analyses carried out under operating conditions of acceleration voltage of 30 kV and a 120 μm aperture. Mineral compositions were determined at the Inter-Institution Laboratory of Microanalysis of Minerals and Synthetic Substances (Faculty of Geology, University of Warsaw), using a Cameca SXFiveFE electron probe micro analyser (EPMA) equipped with five wavelength dispersive spectrometers (WDS). The operating conditions of the electron microprobe were: 15 kV accelerating voltage, 6–20 nA probe current and focused or defocused (3–10 μm in diameter) electron beam. The φ(ρZ) correction model (X-PHI in the electron microprobe software) developed by Merlet (1994) was used for corrections. All the standards, lines etc. used are listed in the Appendices to Tables 2 and 3. Due to changes in the analysis conditions, applied in order to acquire data of highest possible quality, the detection limits in the Appendices are expressed as ranges instead of exact values. The locations of the analysed spots are shown in the Supplementary Material (Fig. S1) – available only in the online version.

Prior to the EBSD examination, the sample was additionally polished (using a vibrating polisher)

	Henrymeyerite						Fe-poor Ba titanate			
	1	2	3	6	9	11	19	21	27	31
Anal. no.	IL-379	IL-380	IL-381	IL-407	IL-410	IL-417	IL-389	IL-392	IL-399	IL-404
BaO	17.65	17.25	17.07	16.94	18.28	18.72	20.03	20.36	20.63	25.86
CaO	0.14	0.10	0.04	0.74	0.13	0.14	bd	bd	bd	bd
Na ₂ O	0.27	0.33	0.34	0.18	bd	bd	0.03	0.15	0.37	0.03
K ₂ O	bd	0.04	0.04	0.03	bd	0.03	bd	0.03	0.03	0.03
La ₂ O ₃	0.37	0.38	0.38	0.35	0.38	0.38	0.43	0.39	0.41	0.40
Ce ₂ O ₃	0.33	0.39	0.33	0.53	0.26	0.27	0.46	0.35	0.40	0.43
TiO ₂	70.18	69.98	69.81	69.04	71.50	71.06	75.88	75.70	73.70	71.84
FeO*	9.40	9.17	9.49	9.49	9.29	10.08	1.10	1.52	1.38	2.73
MnO	bd	0.08	0.09	0.07	bd	0.05	bd	0.07	0.07	bd
MgO	bd	bd	bd	bd	bd	bd	bd	bd	bd	bd
Nb ₂ O ₅	0.61	0.96	0.46	1.63	bd	bd	1.09	1.03	1.16	0.19
SiO ₂	0.59	0.93	1.10	0.29	bd	bd	0.10	0.22	1.13	0.07
Total	99.54	99.61	99.15	99.29	99.84	100.73	99.12	99.82	99.28	101.58
Formula on the basis of 16 oxygens										
Ba	0.900	0.875	0.869	0.868	0.932	0.953	0.692	0.700	0.714	0.919
Ca	0.020	0.014	0.006	0.104	0.018	0.019	0.000	0.000	0.000	0.000
Na	0.068	0.083	0.086	0.046	0.000	0.000	0.005	0.026	0.063	0.005
K	0.000	0.007	0.007	0.005	0.000	0.005	0.000	0.003	0.003	0.003
La	0.018	0.018	0.018	0.017	0.018	0.018	0.014	0.013	0.013	0.013
Ce	0.016	0.018	0.016	0.025	0.012	0.013	0.015	0.011	0.013	0.014
Ti	6.865	6.814	6.817	6.789	6.996	6.939	5.028	4.996	4.895	4.898
Fe ²⁺	1.023	0.993	1.031	1.038	1.011	1.095	0.081	0.112	0.102	0.207
Mn	0.000	0.009	0.010	0.008	0.000	0.005	0.000	0.005	0.005	0.000
Mg	0.000	0.000	0.000	0.000	0.000	0.000	0.000	0.000	0.000	0.000
Nb	0.036	0.056	0.027	0.096	0.000	0.000	0.043	0.041	0.046	0.008
Si	0.077	0.120	0.143	0.038	0.000	0.000	0.009	0.019	0.100	0.006
Σ cations	9.02	9.01	9.03	9.03	8.99	9.05	5.89	5.93	5.96	6.07

Table 2. Representative compositions of Ba-Fe titanates (in wt.%). FeO* – all Fe as Fe²⁺; bd – below detection.

	1	2	3	4	5	6	7
Anal. no.	IL-382	IL-383	IL-384	IL-391	IL-398	IL-401	IL-456
Na ₂ O	0.11	2.80	0.08	4.51	1.91	1.53	0.05
CaO	0.44	0.06	bd	bd	bd	bd	0.08
BaO	27.56	28.44	30.12	17.88	22.03	25.25	20.17
La ₂ O ₃	0.29	0.24	0.30	0.23	0.27	0.32	0.25
Ce ₂ O ₃	0.40	0.31	0.71	bd	0.37	0.54	0.42
Al ₂ O ₃	0.08	0.08	bd	bd	bd	bd	bd
TiO ₂	48.19	46.92	55.17	47.17	46.75	52.27	49.09
FeO*	7.06	3.19	2.23	13.04	11.71	4.89	15.54
MnO	0.23	0.11	0.14	1.85	1.10	0.46	1.47
MgO	bd						
Nb ₂ O ₅	3.51	2.67	0.89	1.10	1.01	1.05	1.27
SiO ₂	11.25	14.25	9.51	13.45	11.83	10.59	8.25
Cl		1.52	1.40	1.09	1.26	1.16	1.11
Sum	99.12	100.59	100.55	100.32	98.24	98.06	97.70
O ≡ Cl		0.35	0.32	0.25	0.29	0.27	0.25
Total	99.12	100.24	100.23	100.07	97.95	97.79	97.45

Table 3. Compositions of unidentified Ba titanosilicate (in wt.%). FeO* – all Fe as Fe²⁺; bd – below detection; blank – not determined.

for 8 hours in a diamond suspension with a grain diameter of 1/4 micron. The sample was covered with a 4.3 nm carbon layer for better surface discharge EBSD patterns were collected with a Zeiss Auriga electron microscope equipped with a Bruker e – FlashHR+ detector with integrated ARGUS imaging device. The sample was tilted to 70° using the dedicated stage (tilt about sample X axis) for an optimal EBSD signal, while the detector tilt angle was 1.25° and sample to detector distance of 15.66 mm. The experiment was carried out using an electron beam with energy of 15 keV. Image tilt correction was used on the Zeiss SmartSEM software and no image rotation was applied. A single EBSD pattern of 400 × 300 resolution was recorded from the 0.39 × 0.39 micrometer area during 300 ms. The system was calibrated in Bruker ESPRIT 2. The pattern centre (PC), in Bruker fractional coordinates, was measured as: $PC_x = 0.489$, $PC_y = 0.237$ with a pattern aspect ratio of 1.33 (width/height), detector distance 15.45 mm.

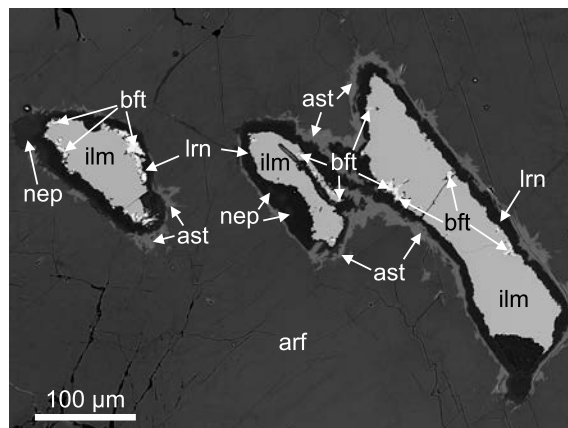
OCCURRENCE OF HENRYMEYERITE AND ASSOCIATED MINERALS

Textural details of the henrymeyerite, Fe-poor Ba titanate and unidentified Ba titanate are shown in Text-fig. 2. Three grains of ilmenite (Text-fig. 1), the largest of which is ~340×60 μm in size, are enclosed in an arfvedsonite crystal. The ilmenites appear to have been partially resorbed and then mantled by a layer of lorenzenite ~10–30 μm thick (Text-fig. 2A). The lorenzenite was in turn mantled by a thin layer of astrophyllite, varying in width from 5 to 20 μm, which sent thin branches into the arfvedsonite. Neptunite is intergrown with, and patchily replaces, the lorenzenite (Text-fig. 2B). The Ba titanates locally form little clusters fringing the ilmenite grains (Text-fig. 2C). They are mainly acicular, up to 10 μm long, but also form small patches. In Text-fig. 2D, an unidentified Ba titanate accompanies the titanate.

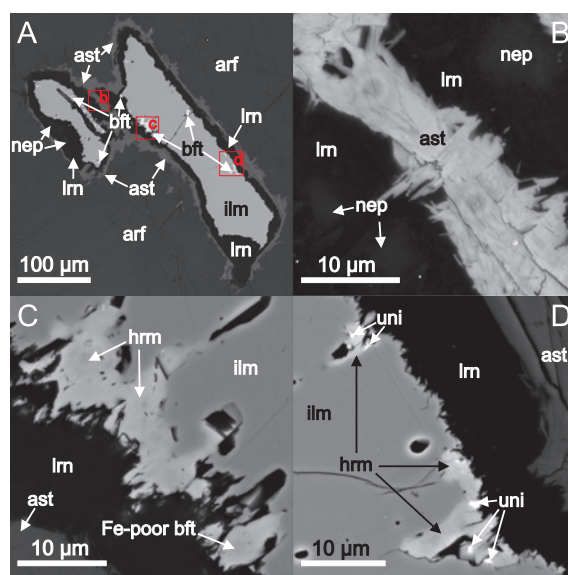
MINERAL COMPOSITIONS

Ba titanates

There are two compositional varieties (Table 2; Supplementary Table S1a). One is a Ba-Fe titanate, with the average formula ($n = 17$) $[(Ba_{0.92}Na_{0.05}Ca_{0.03})_{1.0}$

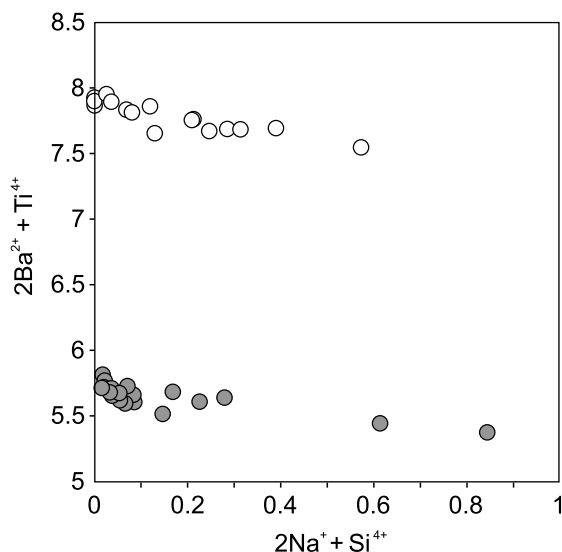


Text-fig. 1. BSE image of ilmenite (ilm) inclusions in arfvedsonite (arf), showing the zones of replacement. Abbreviations: lrm – lorenzenite; ast – astrophyllite; nep – neptunite; bft – Ba-Fe titanates.



Text-fig. 2. A – BSE image showing the mantles of lorenzenite (lrm) and astrophyllite (ast) on ilmenite (ilm) located within arfvedsonite crystal (arf). Henrymeyerite and Fe-poor Ba titanate form clusters (bft) of bright crystals at the edges of the ilmenite. Boxes mark the positions of (B), (C) and (D). B – Neptunite (nep) intergrown with lorenzenite and also patchily replacing it (difficult to discern at the contrast used here). C – Cluster of henrymeyerite (hmm) and Fe-poor Ba titanate (Fe-poor bft). D – Cluster of henrymeyerite (hmm) and an unidentified Ba titanate (uni).

$(Ti_{6.87}Fe^{2+}_{1.04}Nb_{0.03})_{7.9}O_{16}]$. This is henrymeyerite (Mitchell *et al.* 2000). The main component in the A site is Ba (0.79–0.97 a.p.f.u.), with lesser amounts of Ca (0.01–0.07 a.p.f.u.) and Na (b.d.–0.12 a.p.f.u.). La+Ce contents are in the range 0.02–0.04 a.p.f.u.. Titanium dominates the M site (6.67–7.01 a.p.f.u.), with significant amounts of Fe (0.96–1.11 a.p.f.u.) and



Text-fig. 3. Plots of $(\text{Na}^+ + \text{Si}^{4+})$ against $(\text{Ba}^{2+} + \text{Ti}^{4+})$ for henrymeyerite (white circles) and Fe-poor Ba titanate (grey circles). Analyses were based on 16 oxygens (henrymeyerite) and 11 oxygens (Fe-poor Ba titanate). Data source – Supplementary Table S1a.

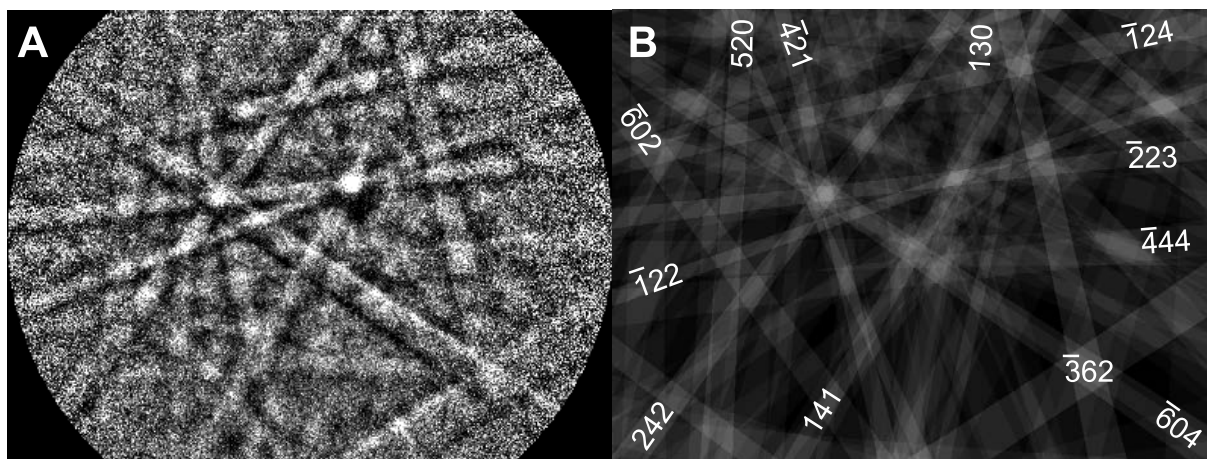
in some analyses Nb (bd–0.10 a.p.f.u.). The close approach to the ideal formula suggests that the Fe is present dominantly as Fe^{2+} , with a very little proportion of the hexatitanate end-member, $\text{BaFe}^{3+}_2\text{Ti}_6\text{O}_{16}$. The entry of Na and Si into the phase may be represented by the substitution $2\text{Na}^+ + \text{Si}^{4+} \rightarrow \text{Ba}^{2+} + \text{Ti}^{4+}$ (Text-fig. 2A).

The second variety in the Green Granite has a much lower Fe content (1.10–2.85 wt.% FeO^* , where FeO^* is all Fe as Fe^{2+}) (Table 2, Appendix to Table 2). Mitchell and Vladykin (1993) reported

an Fe-poor Ba titanate forming reaction mantles on magnetite in aegirine-potassium feldspar syenites from the Little Murun complex, Yakutia, Russia, and suggested that its formula was $(\text{Ba},\text{K})(\text{Ti},\text{Fe})_5\text{O}_{11}$. On the basis of 11 oxygens, the formula of the Green Granite phase can be written ($n = 19$): $[(\text{Ba}_{0.74}\text{Ca}_{0.02}\text{Na}_{0.05})_{0.8}(\text{Ti}_{4.90}\text{Fe}^{2+}_{0.15}\text{Nb}_{0.04})_{5.1}\text{O}_{11}]$, comparable to the Little Murun phase but with lower Fe/Ti ratios, 0.02–0.05 as opposed to 0.05–0.19 and with no replacement of Ba by K. These appear to be the lowest Fe/Ti ratios yet recorded in a natural Ba-Fe titanate. A subset of crystals, brighter on BSE images, have higher Si and Na contents, suggesting perhaps a substitution $2\text{Na}^+ + \text{Si}^{4+} \rightarrow \text{Ba}^{2+} + \text{Ti}^{4+}$, as in henrymeyerite (Text-fig. 3). The nature of the deficiency in the A site is uncertain but may reflect the presence of vacancies. The phase is potentially a new mineral – and although its small size ($\leq 10 \mu\text{m}$) and the fact that it is intergrown with henrymeyerite has made a structural determination very difficult – we managed to acquire EBSD data shown in Text-fig. 4.

Unidentified Ba-Ti-Fe silicate

The unidentified phase associated with the Ba titanates (Table 3) has some compositional affinities with baotite, $\text{Ba}_4\text{Ti}_8\text{Si}_4\text{O}_{28}\text{Cl}$, but there are critical differences. On the basis of 16 cations pfu, there are major deficiencies in Ba (plus Na, K, Ca and REE: 1.9–3.8 a.p.f.u.) and Si (1.9–3.2 a.p.f.u.), and a large excess of Ti (plus Fe, Nb, Mn: 9.2–12.3 a.p.f.u.). The Cl values (0.10–0.59 a.p.f.u.) are far below the stoichiometric 1 a.p.f.u. for baotite. The analyses are very variable; e.g. TiO_2 varies from 46.75 to 55.17 wt.%, FeO^* from 2.23 to 15.54 wt.%, and Nb_2O_5 from 0.89 to 3.51 wt.%.



Text-fig. 4. A representative EBSD pattern from area no. 402 (A) and corresponding simulated pattern of $\text{Ba}_2\text{Ti}_3\text{Nb}_4\text{O}_{18}$ phase with indexed Kikuchi lines (B) that are also visible on the experimental pattern.

The nature of this phase is enigmatic. It is unlikely to be a result of analytical problems: it was analyzed in the same runs as henrymeyerite, which gave satisfactory results. It may have formed by the breakdown of the low-Fe Ba titanate: e.g., $\text{BaTi}_5\text{O}_{11} + \text{Si}^{4+} + 2\text{O}^{2-} \rightarrow \text{BaTi}_3\text{SiO}_9 + 2\text{TiO}_2$, but rutile has not been identified. At this stage we refer to it simply as an unidentified Ba titanosilicate.

A diffraction pattern from polished thin sections around areas 385, 392 and 402 for which, among others compositional analysis indicated low Fe (see Supplementary Table S1a) was captured for Electron Backscatter Diffraction (EBSD) analysis.

For the identification of the barium titanium oxide phase, the crystal structure of $\text{BaTi}_5\text{O}_{11}$ phase, (Tillmanns 1969), crystallizing in a monoclinic system, space group $P2_1/n$ was downloaded from Inorganic Crystal Structure database (ICSD no 26174), and uploaded to the ESPRIT software database to be included in EBSD patterns identification. The collected patterns were compared to theoretical, simulated Kikuchi lines generated by the Esprit software. No match to the known $\text{BaTi}_5\text{O}_{11}$ (Tillmanns 1969) crystal structure was found in the analyzed areas of the sample. Further search was initiated for any phases containing oxygen, titanium and any other elements. A very good match (Text-fig. 4B) of the experimentally registered Kikuchi lines was found with a phase of the formula $\text{Ba}_2\text{Ti}_3\text{Nb}_4\text{O}_{18}$ crystallizing in the monoclinic system, space group $P2_1/c$ (Gasparin 1984). It is plausible that the studied barium titanate of formula $\text{BaTi}_5\text{O}_{11}$ has a new and yet unknown crystal structure or its chemical formula is different, where the end-member is $\text{Ba}_2\text{Ti}_7\text{O}_{18}$.

FORMATION OF THE BA TITANATES

Our ongoing studies of the textural relationships in the Green Granite indicate that the accessory minerals formed over a range of conditions, from early- to late-magmatic and hydrothermal. A continuous transition from melt to fluid resulted in extensive autometasomatism and hydrothermal overprints. Early mineral assemblages were therefore partially replaced to various extents by late-magmatic phases formed from a volatile-saturated melt and then by secondary minerals from hydrothermal fluids during a late deuteric stage.

Given their occurrence as fringes of tiny crystals on ilmenite grains, the Ba titanates are probably of hydrothermal origin. A hydrothermal origin was reported for the type henrymeyerite by

Mitchell *et al.* (2000). Similarly, Chakmouradian and Mitchell (1999) recorded Ba titanate forming, with ilmenite, rims on rutile in nepheline syenite pegmatites at Pegmatite Peak, Bearpaw Mountains, Montana, ascribing it to late-stage deuteric alteration. Chakmouradian and Mitchell (2002) found Ba-Fe titanates formed by deuteric alteration of nepheline syenites from the Crazy Mountains, Montana. In the Šebkovice dyke, Czech Republic, henrymeyerite occurs in aggregates in late-stage titanite veinlets (Krmíček *et al.* 2011). The phase $\text{BaTi}_5\text{O}_{11}$ has also been synthesized experimentally. Using as starting materials barium acetate $[\text{Ba}(\text{CH}_3\text{COO})_2]$ and tetrabutyl titanate $[\text{Ti}(\text{C}_4\text{H}_9\text{O})_4]$, and with NaOH as a pH-adjusting agent in the aqueous precursor, Li *et al.* (2019) synthesized $\text{BaTi}_5\text{O}_{11}$ nanocrystals at 280 °C in 20 h. The Green Granite occurrence is entirely consistent with these natural and experimental parageneses.

A significant problem in attempting to estimate the crystallization conditions of the titanates is the petrographic complexity of the granite. For example, our sample contains 26 accessory minerals, each potentially able to provide information on their conditions of formation. Here we comment briefly on certain parameters. Marks *et al.* (2003) proposed, on the basis of phase equilibria, that the formation of the accessories in the peralkaline granite of the Gardar Puklen complex formed at temperatures as low as 300 °C with progressive increases in $f\text{O}_2$. For example, aegirine replaced arfvedsonite at $T < 300$ °C and at an $f\text{O}_2$ above the hematite-magnetite (HM) buffer. For the Green Granite, that temperature estimate is consistent with the 280 °C found during synthesis of $\text{BaTi}_5\text{O}_{11}$ (Li *et al.* 2019). The oxidized conditions are not, however, reflected in the Fe^{3+} -poor nature of the henrymeyerite inferred in this study.

Mineral formation in the later stages of the Green Granite took place in the presence of fluids. Konnerup-Madsen and Rose-Hansen (1984) showed that fluid inclusions in quartz in the granite were entirely aqueous, with salinities from about 2 to 64 wt.%. Melt water contents are more difficult to estimate. In experimental studies of pantellerites, Scaillet and Macdonald (2003) and Di Carlo *et al.* (2010) showed that there is a positive correlation between CaO in amphibole and melt water content. Applying the relationship to the Green Granite is hampered by the fact that the arfvedsonites show a range of CaO contents, 0.5–2.0 wt.% (our unpublished data). That range, however, indicates a maximum water content of ~2 wt.%; such a low value suggests that the melt had partially degassed at the time of titanate crystallization.

Acknowledgements

We thank Adam Pieczka and Bruno Scaillet for very helpful journal reviews. Special thanks to Brian G. J. Upton for providing us with the samples. We also thank Paula Sierpień for help with conversion of the figures. This research was funded by the Faculty of Geology KGMiP grant 501 D-113 01 113 01 00.

REFERENCES

- Biagioni, C., Capalbo, C. and Pasero, M. 2013. Nomenclature tunings in the hollandite supergroup. *European Journal of Mineralogy*, **25**, 85–90.
- Chakmouradian, A.R. and Mitchell, R.H. 1999. Primary, apatitic and deuteric stages in the evolution of accessory Sr, REE, Ba and Nb mineralization in nepheline-syenite pegmatites at Pegmatite Peak, Bearpaw Mts, Montana. *Mineralogy and Petrology*, **67**, 85–110.
- Chakmouradian, A.R. and Mitchell, R.H. 2002. The mineralogy of Ba- and Zr-rich alkaline pegmatites from Gordon Butte, Crazy Mountains (Montana, USA): comparisons between potassic and sodic apatitic pegmatites. *Contributions to Mineralogy and Petrology*, **143**, 93–114.
- Di Carlo, I., Rotolo, S.G., Scaillet, B., Buccheri, V. and Pichavant, M. 2010. Phase equilibrium constraints on pre-eruptive conditions of recent felsic explosive volcanism at Pantelleria Island, Italy. *Journal of Petrology*, **51**, 2245–2276.
- Gasparin, M. 1984. Synthèse et structure d'un nouveau titanoniobate: le trititanotétraniobate de dibaryum, $\text{Ba}_2\text{Ti}_3\text{Nb}_4\text{O}_{18}$. *Acta Crystallographica Section C: Crystal Structure Communications*, **40**, 9–11.
- Konnerup-Madsen, J. and Rose-Hansen, J. 1984. Composition and significance of fluid inclusions in the Ilímaussaq peralkaline granite, South Greenland. *Bulletin de Minéralogie*, **107**, 317–326.
- Krmíček, L., Cempírek, J., Havlin, A., Přichystal, A., Houzar, S., Krmíčková, M. and Gadas, P. 2011. Mineralogy and petrogenesis of a Ba-Ti-Zr-rich peralkaline dyke from Šebkovice (Czech Republic): Recognition of the most lamproitic Variscan intrusion. *Lithos*, **121**, 74–86.
- Krumrei, T.V., Villa, I.M., Marks, M. and Markl, G. 2006. A $^{40}\text{Ar}/^{39}\text{Ar}$ and U/Pb isotopic study of the Ilímaussaq complex, South Greenland: implications for the ^{40}K decay constant and for the duration of magmatic activity in a peralkaline complex. *Chemical Geology*, **227**, 258–273.
- Li, S., Li, X., Zou, K., Huang, Z., Zhang, L., Zhou, X., Guo, D., Ju, Y. 2019. Preparation of single-crystalline $\text{BaTi}_5\text{O}_{11}$ nanocrystals by hydrothermal method. *Materials Letters*, **245**, 215–217.
- Marks, M.A.W., Vennemann, T., Siebel, W. and Markl, G. 2003. Quantification of magmatic and hydrothermal processes in a peralkaline syenite-alkali granite complex based on textures, phase equilibria, and stable and radiogenic isotopes. *Journal of Petrology*, **44**, 1247–1280.
- Merlet, C. 1994. An accurate computer correction program for quantitative electron probe microanalysis. *Microchimica Acta*, **114/115**, 363–376.
- Mikhailova, Y.A., Konopleva, N.G., Yakovenchuk, V.N., Ivanjuk, G.Y., Men'shikov, Y.P. and Pakhomovsky, Y.A. 2007. Corundum-group minerals in rocks of the Khibiny alkaline plutonic complex, Kola Peninsula. *Geology of Ore Deposits*, **49** (7), 590–598.
- Mitchell, R.H. and Bergman, S.C. 1991. Petrology of Lamproites, 447 pp. Plenum Press; New York.
- Mitchell, R.H. and Vladykin, N.V. 1993. Rare earth element-bearing tausonite and potassium barium titanates from the Little Murun potassic alkaline complex, Yakutia, Russia. *Mineralogical Magazine*, **57**, 651–664.
- Mitchell, R.H., Yakovenchuk, V.N., Chakmouradian, A.R., Burns, P.C. and Pakhomovsky, Y.A. 2000. Henrymeyerite, a new hollandite-type Ba-Fe titanate from the Kovdor complex, Russia. *The Canadian Mineralogist*, **38**, 617–626.
- Nielsen, B.L. and Steenfelt, A. 1978. Intrusive events at Kvanefjeld in the Ilímaussaq igneous complex. *Bulletin of the Geological Society of Denmark*, **27**, 143–155.
- Platt, R.G. 1994. Perovskite, loparite and Ba-Fe hollandite from the Schryburt Lake carbonatite complex, northwestern Ontario, Canada. *Mineralogical Magazine*, **58**, 49–57.
- Scaillet, B. and Macdonald, R. 2003. Experimental constraints on the relationships between peralkaline rhyolites of the Kenya Rift Valley. *Journal of Petrology*, **94**, 1867–1894.
- Steenfelt, A. 1981. Field relations in the roof zone of the Ilímaussaq intrusion with special reference to the position of the alkali acid rocks. *Rapport Grønlands Geologiske Undersøgelse*, **103**, 43–52.
- Tillmanns, E. 1969. Die Kristallstruktur von $\text{BaTi}_5\text{O}_{11}$. *Acta Crystallographica Section B: Structural Crystallography and Crystal Chemistry*, **25**, 1444–1452.
- Upton, B.G.J. 2013. Tectono-magmatic evolution of the younger Gardar southern rift, South Greenland. *Geological Survey of Denmark and Greenland Bulletin*, **29**, 1–124.

APPENDIX (to Table 2)

15 nA beam current, focused beam.

Element	Line	Crystal	Standard	Detection limit (wt.%)
Ba	L α	LLIF	BaSO ₄	0.137–0.182
Ca	K α	LPET	wollastonite	0.012
Na	K α	TAP	sodalite	0.039–0.047
K	K α	LPET	orthoclase	0.016–0.018
La	L α	LPET	LaPO ₄	0.050–0.053
Ce	L α	LPET	CePO ₄	0.001–0.007
Ti	K α	LLIF	TiO ₂	0.049–0.067
Fe	K α	LLIF	hematite	0.053–0.065
Mn	K α	LLIF	rhodonite	0.049–0.053
Mg	K α	LTAP	MgO	0.014
Nb	L α	LPET	Nb metal	0.052–0.059
Si	K α	TAP	wollastonite	0.020–0.022

APPENDIX (to Table 3)

10–15 nA beam current, focused beam.

Element	Line	Crystal	Standard	Detection limit (wt.%)
Na	K α	TAP	sodalite	0.044–0.062
Ca	K α	LPET	wollastonite	0.013–0.015
Ba	L α	LLIF	BaSO ₄	0.171–0.230
La	L α	LPET	LaPO ₄	0.052–0.064
Ce	L α	LPET	CePO ₄	0.003–0.007
Al	K α	TAP	orthoclase	0.029–0.036
Ti	K α	LLIF	TiO ₂	0.062–0.080
Fe	K α	LLIF	hematite	0.064–0.077
Mn	K α	LLIF	rhodonite	0.051–0.063
Mg	K α	LTAP	MgO	0.015
Nb	L α	LPET	Nb metal	0.058–0.073
Si	K α	TAP	wollastonite	0.021–0.026
Cl	K α	LPET	sodalite	0.020–0.023